Archives of Acoustics Vol. 48, No. 4, pp. 593–601 (2023), doi: 10.24425/aoa.2023.146644

Research Paper

Removal of Fouling from Steel Plate Surfaces Based on Multi-Frequency Eco-Friendly Ultrasonic Guided Wave Technology

Mingkun HUANG(1), Shuo JIN(2), Gaoqian NIE(1), Xiaopeng WANG(1), Quanpeng ZHANG(1), Yang AN(1),(3), Zhigang QU(1),(3)*, Wuliang YIN(4)

(1) *College of Electronic Information and Automation*
Tianjin University of Science and Technology
Tianjin, China

(2) *School of Electrical and Information Engineering, Tianjin University*
Tianjin, China

(3) *Advanced Structural Integrity International Joint Research Centre*
Tianjin University of Science and Technology
Tianjin, China

(4) *School of Electrical and Electronic Engineering, University of Manchester*
Manchester, United Kingdom

*Corresponding Author e-mail: zhigangqu@tust.edu.cn

(*received September 15, 2022; accepted April 14, 2023*)

Fouling is inevitable on the surfaces of industrial equipment, especially on heat-exchanging surfaces in contact with fluids, which causes water pollution and destroys the ecological environment. In this paper, a novel fouling-removal methodology for plate structure based on cavitation by multi-frequency ultrasonic guided waves is proposed, which can remove fouling on stainless steel plates. A numerical simulation method has been developed to study the acoustic pressure distribution on a steel plate. According to the simulation results, the distribution of sound pressure on the plate under triple-frequency excitation is denser and more prone to cavitation than in single-frequency cases and dual-frequency cases, which improves fouling removal rate. The stainless steel plate is immersed in water for the descaling experiment, and the results show that the fouling removal rates of three water-loaded stainless steel plates under different single-frequency excitation seem unsatisfactory. However, the multi-frequency excitation improves the descaling performance and the removal rate of fouling reaches 80%. This new method can be applied to the surface descaling of large equipment plates, which is of great significance for purifying water quality and protecting the ecological environment.

Keywords: fouling removal; cavitation; eco-friendly; ultrasonic guided waves; multi-frequency.

1. Introduction

Fouling is easy to deposit on the inner surfaces of industrial equipment due to long-term contact with the liquid medium. The industrial equipment includes boilers, chillers, and membrane filtration systems in which the heat exchanger part easily produces fouling, especially calcium carbonate (Somerscales, 1990). Fouling reduces thermal conductivity leading to a decrease in production capacity and an increase in energy consumption. Furthermore, some unexpected mechanical breakdowns may be incurred due to fouling, consequently causing financial loss and even severe industrial accidents (Abu-Zaid, 2000).

Traditional methods of descaling on the surface of industrial equipment mainly include a mechanical method, hydro-blasting method, chemical method, and ultrasonic method (Kudryashova *et al.*, 2019; Gholivand *et al.*, 2010; Krzyzanowski *et al.*, 2013; Mason, 2016). The ultrasonic method, dating from the

middle of the 20th century, has become a mainstream approach for cleaning, which is capable of removing surface fouling based on the acoustic cavitation effect (Legay *et al.*, 2013; Deptuła *et al.*, 2016; Mason, 2016). In traditional ultrasonic cleaning methods, the transducers are attached to the bottom of the water tank with cleaning fluid, generating high-frequency mechanical vibrations to clean the objects immersed in the fluid through ultrasound cavitation (Kim *et al.*, 1999; Wu, Chao, 2011).

Ultrasonic guided waves (UGWs) technique has been widely used in structural health monitoring (SHM). In recent years, UGWs techniques have also been used to remove fouling on structures (Habibi *et al.*, 2016). In our previous study, a new approach to pipeline descaling based on leaky-guided ultrasonic wave cavitation was proposed, and the experiment results showed that the new approach had high efficiency in removing fouling in the water-filled pipe (Qu *et al.*, 2019). According to these findings, the UGWs have the potential for long-distance fouling removal because they can propagate a longer distance than traditional ultrasound. At the same time, this technique allows for non-stop operation, enabling continuous fouling removal. Additionally, the use of UGWs for fouling removal can significantly reduce maintenance costs.

Cavitation is an essential principle used in descaling. When UGWs propagate along a structure with a liquid load, a part of the energy will leak into the liquid through the solid-liquid boundary, which can cause liquid cavitation. The cavitation induced by ultrasonic waves can be used to clean solid surfaces and remove scale (Pečnik *et al.*, 2016; Shchukin *et al.*, 2011). In recent years, multi-frequency ultrasound has been reported to improve the ultrasonic cavitation effect (Feng *et al.*, 2002; Suo *et al.*, 2018; Avvaru, Pandit, 2008). Twenty-kilohertz ultrasound was applied to a cross-flow ultrafiltration system with alumina membranes. The ultrasonic control of membrane fouling caused by silica particles was investigated under various solution conditions (Chen *et al.*, 2006).

This paper mainly discusses the effect of the descaling on stainless steel plates using multi-frequency UGWs. The descaling effect on stainless steel plate under the same power and different frequency combination excitation is studied and analyzed. Meanwhile, a curve graph of the descaling rate with the corresponding descaling time is shown.

2. Theory

When the wave propagates in a bounded medium, solid boundaries can guide the propagation of waves in the form of reflection and refraction. The guided waves in the plate can be regarded as a superposition of waves led by bulk wave reflection and refraction at the upper and lower boundary of a plate (Zhu *et al.*, 2011). As the waves propagate along a plate with liquid loading, part of the energy leaks into liquid. A new descaling method based on UGWs for plates is proposed, as shown in Fig. 1.

For any isotropic medium, the displacement vector $\mathbf{U}$ of UGW in the plate satisfies the Navier displacement equation of motion (Rizzo, Shippy, 1971; Kovarik, 1995; Mazzotti *et al.*, 2014), which can be expressed as Eq. (1). Using Helmholtz decomposition, the displacement vector field can be expressed as the gradient of a scalar $\mathbf{\Phi}$ and the curl of a vector $\boldsymbol{\psi}$, as Eq. (2):

$$(\lambda+\mu)\nabla\nabla\cdot\mathbf{U}+\mu\nabla^2\mathbf{U}=\rho\cdot\left(\partial^2\mathbf{U}/\partial t^2\right), \tag{1}$$

$$\mathbf{U}=\nabla\mathbf{\Phi}+\nabla\times\boldsymbol{\psi}, \tag{2}$$

where λ and $\mathbf{U}$ are Lame's constants of an elastic isotropic solid, and ρ is the density.

When the plate surface is loaded with water, it provides a path for UGWs energy leakage. If the phase velocity of the UGWs in the plate is greater than in the fluid, energy will leak into the fluid (Inoue, Hayashi, 2015). So the waves attenuate as they propagate in the plate, and the displacement is

$$\mathbf{U}=A_a e^{i(k_r x-\omega t)}e^{-\alpha x}, \tag{3}$$

where A_a is the amplitude of the wave in the plate, k is the wave number, and α is the decay factor.

Because shear stress cannot propagate in the liquid, vector potential is equal to zero. When longitudinal waves propagate in the water, the potential function $\mathbf{\Phi}$ should be considered together with an additional displacement field equation (Sato *et al.*, 2007).

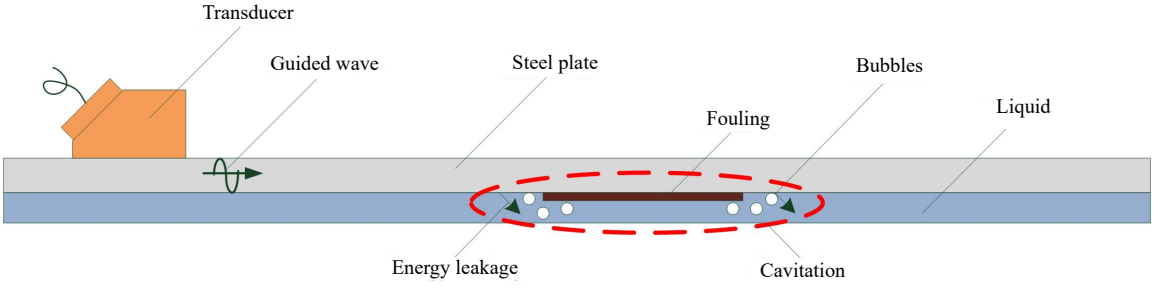

Fig. 1. Propagation direction of UGWs and the descaling principle of leakage UGWs on the steel plate.

The displacement **U** in water by leaky UGWs can be expressed as the gradient of a scalar **Φ**:

$$\mathbf{U} = \nabla \mathbf{\Phi}, \tag{4}$$

$$\mathbf{\Phi} = A_l e^{-ik_l y} e^{i(kx-\omega t)}, \tag{5}$$

$$k_l = \sqrt{(\omega/c_l)^2 - k^2}, \tag{6}$$

where A_l is the amplitude of wave in the liquid, k is the wave number, and c_l is the longitudinal wave velocity in the liquid.

UGWs leaking into the liquid cause a cavitation effect. If the amplitude of acoustic pressure is higher than the cavitation threshold, the bubbles in liquid will expand under negative pressure and absorb a lot of energy from the sound field, compress and collapse sharply under positive pressure, resulting in high temperature and high pressure (Suslick *et al.*, 1999), which will effectively remove the fouling on the plate. The cavitation threshold is defined as the minimum amplitude of sound pressure required to initiate acoustic cavitation (Nguyen *et al.*, 2017), which can be expressed as:

$$P_b = P_0 - P_V + \frac{2}{3\sqrt{3}}\left[\left(\frac{2\sigma}{R_0}\right)^3 \Big/ \left(P_0 - P_V + \frac{2\sigma}{R_0}\right)\right]^{1/2}, \tag{7}$$

where P_b is the cavitation threshold, P_0 is the hydrostatic pressure, P_V is the saturated vapor pressure, R_0 is the initial radius of a bubble, and σ is the tension coefficient of the liquid.

When the external driving sound pressure exceeds the cavitation threshold, not all bubbles will collapse. The cavitation effect occurs only when the ultrasonic frequency is less than the resonant frequency of the bubble or the initial radius of the bubble is smaller than the resonant radius. Otherwise, the cavitation bubble has nonlinear vibration. The resonant frequency of the bubble (Shima *et al.*, 1971) can be expressed as:

$$f_r = \frac{1}{2\pi R_0}\sqrt{\left[\frac{\gamma}{\rho}\left(p_0 + \frac{2\sigma}{R_0}\right) - \frac{2\sigma}{\rho R_0}\right]}, \tag{8}$$

where γ is the specific heat ratio, ρ is the liquid density, and f_r is the resonant frequency.

3. Simulation

Based on the theory presented in Sec. 2, leaky acoustic pressure is a critical factor in determining whether cavitation occurs on the surface of the plate during the descaling process. To study the characteristics of the sound field at different frequencies, finite element simulation is used to understand the acoustic pressure distribution on the plate.

3.1. Model set-up

The model set-up is shown in Fig. 2a, wherein the plate is made of 304 steel material. The plate has a length of 500 mm, a width of 100 mm, and a thickness of 2 mm. On one side of the plate there is layer of $CaCO_3$ that spans a length of 180 mm. The plate is subjected to a water load. Most commonly used ultrasonic testing (UT) angle transducers use methyl polymethacrylate as the body wedge material. In this case and when emitting ultrasound waves to steel, it is possible to operate within the specified incidence angle range of 27.6–57.7° (Krautkrämer, Krautkrämer, 2013). The wedge-shaped transducer consists of PZT-5H piezoelectric material and a square aluminum base. The dimensions of the aluminum base are $85 \times 48 \times 50$ mm, and the dimensions of the piezoelectric sheet are 50 mm outer diameter, 17 mm inner diameter, and 5 mm thickness.

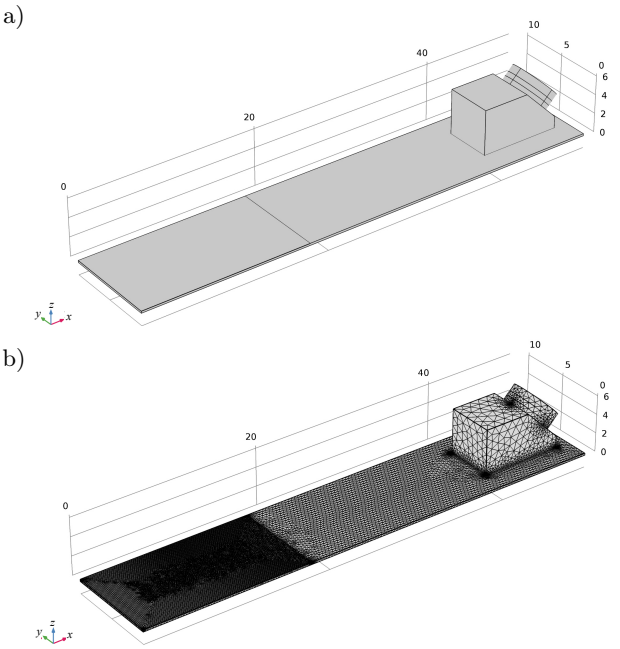

Fig. 2. a) FEM model; b) mesh of the model.

The performance parameters of the transducer-sensitive element PZT as shown in Table 1.

Table 1. PZT parameter of the transducer.

	Radial resonant frequency (f_s)	Radial anti-resonant frequency (f_p)	Transverse electromechanical coupling coefficient (k)	Equivalent capacitance (C)	Elastic modulus (e)	Longitudinal wave velocity (V_l)	Transverse wave velocity (V_t)	Dielectric constant (ε)
Parameter	35 528 Hz	38 200 Hz	0.367	3050 pf	61 Gpa	4500 m/s	2200 m/s	380

The incident angle of the transducer is set at 45°, following the principle of oblique incidence and generating the UGW in the F mode. The transducer is coupled at one end of the plate to ensure that the UGWs energy excited by the transducer can be effectively transmitted. The mesh of the model is presented in Fig. 2b. The region covered with fouling on the plate is the main calculation domain, in which the largest cell size should be less than or equal to the 1/8 minimum wavelength criterion. In Fig. 2b, the mesh of the main calculation domain (region covered with $CaCO_3$ fouling on the plate) is denser than the other parts to ensure calculation accuracy.

3.2. Simulation result

The absolute acoustic pressure results in the region covered with fouling under different frequencies are shown in Fig. 3. The three frequencies with peak acoustic pressure are 24.767, 35.144, and 42.498 kHz, under which the distribution of acoustic pressure on the plate is studied in the simulation.

The absolute acoustic pressure distribution results on the plate under different frequency combinations are shown in Fig. 4.

According to Fig. 4, under single-frequency excitation, the peak distribution of sound pressure on the

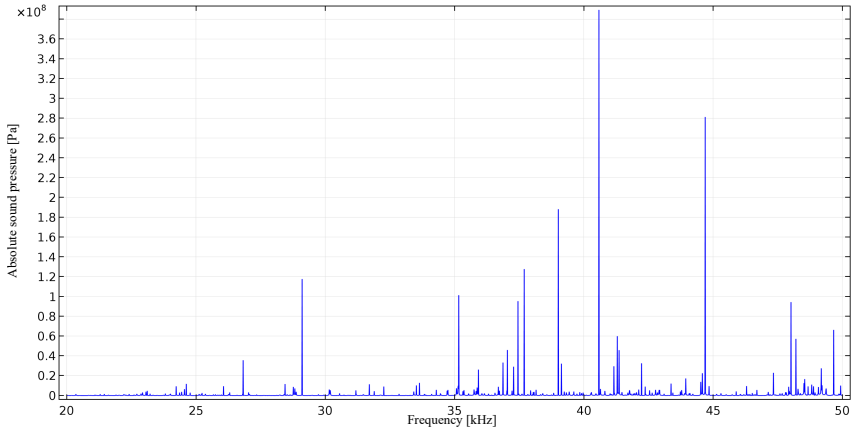

Fig. 3. Absolute acoustic pressure under different frequencies.

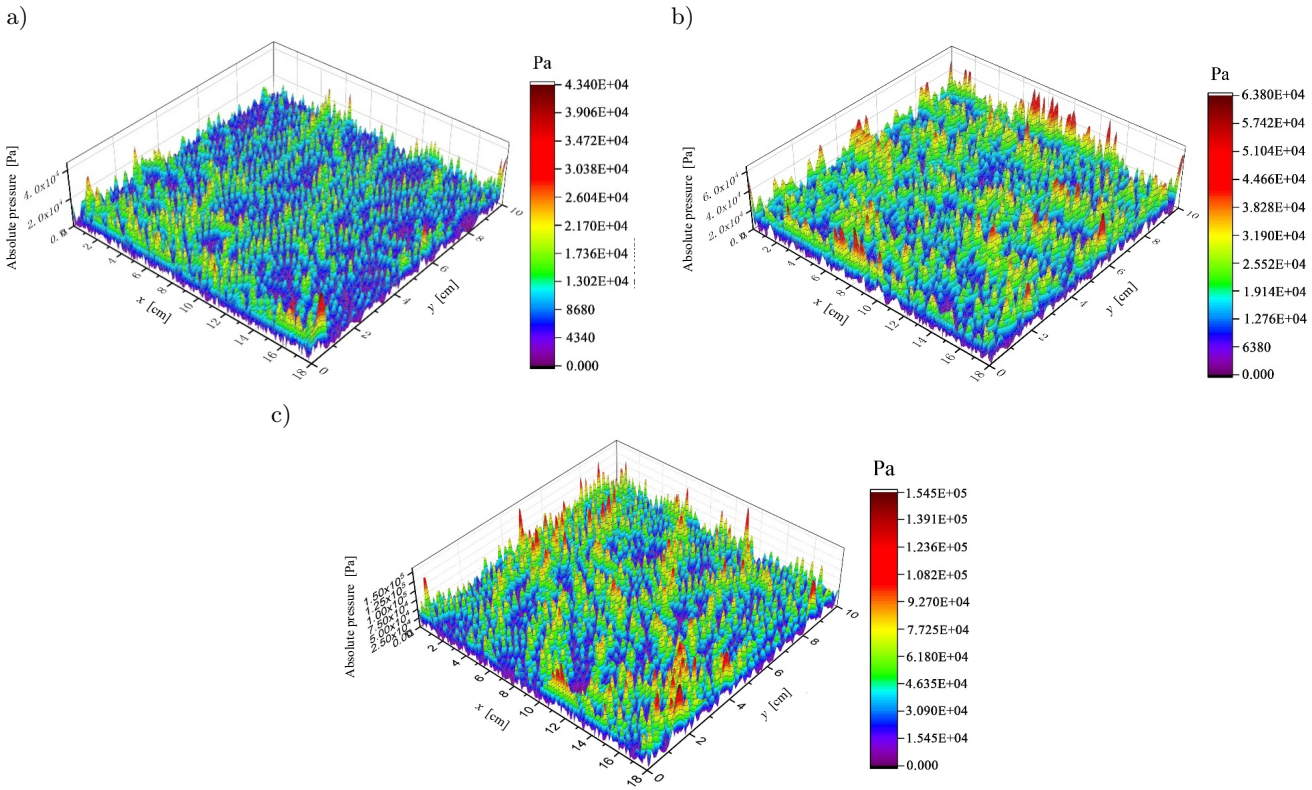

Fig. 4. Absolute sound pressure distribution under different frequency combinations: a) single-frequency 24.767 kHz; b) dual-frequency 24.767 and 35.144 kHz; c) triple-frequency 24.767, 35.144, and 42.498 kHz.

plate is scattered and the overall sound pressure value is relatively low. When the peak value reaches the cavitation threshold, cavitation for descaling occurs. In another way, cavitation for descaling cannot occur in areas where there are low acoustic pressure values. Hence the descaling on the plate under single-frequency excitation is not uniform. Compared with single-frequency excitation, the sound pressure on the plate under dual-frequency and triple-frequency excitation is more densely divided, and the sound pressure value increases. The uniformity of the sound pressure distribution in the triple-frequency mode is similar to that of the dual-frequency mode. However, the sound pressure values are an order of magnitude higher in the triple-frequency mode.

4. Experiments and results

4.1. Transducer testing

A single 45° beam angle transducer is used in this work, as shown in Fig. 5a, which consists of a square base and piezoelectric material. Electric energy is converted to mechanical vibration by a transducer based on the piezoelectric effect and generates UGWs propagation in the plate based on Snell's law.

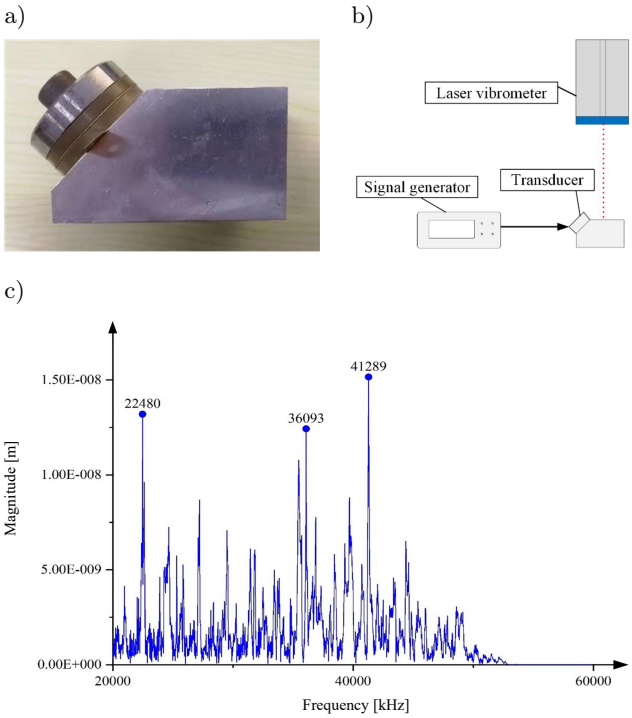

Fig. 5. a) Transducer used in this work; b) transducer testing set-up; c) displacement-frequency characteristic curve of the transducer.

To test the mechanical vibration performance of the transducer at each frequency, the transducer testing system is set up, as shown in Fig. 5b. A pulse signal is generated by the signal generator and input to the transducer. The vibration characteristics of the transducer are obtained by using and reading a laser vibrometer, and the displacement-frequency characteristic curve of the transducer is shown in Fig. 5c.

The calibration results show that the displacement of the transducer reaches three peak values when the frequency is 22.480, 36.093, and 41.289 kHz, where the transducer has a good electrical-acoustic conversion efficiency. To improve the effect of cavitation for descaling, the above three frequencies are selected for the descaling experiments.

4.2. Electrochemical reaction

Calcium carbonate fouling is an intractable topic in industrial fields. Calcium carbonate fouling is easy to generate on the surface of heat-exchange equipment, boiler, and other industrial equipment (MacAdam, Parsons, 2004), and this study mainly focuses on the removal of calcium carbonate fouling on plate surfaces. The system shown in Fig. 5a is designed to generate calcium carbonate fouling on the steel plate.

The output voltage of the power supply is 30 V. The experimental plate is set as the working electrode and connected to the negative electrode of the power supply. The other plate is set as a reference electrode and connected to the positive electrode. Two plates are both dipped in water-nanosized calcium carbonate colloid. The calcium carbonate fouling layer is formed by an electrochemical reaction on the working electrode plate.

Electrochemical reaction experiments are carried out on seven stainless steel plates of the same size: a length of 500 mm, a width of 100 mm, and a thickness of 2 mm. The electrochemical fouling preparation system is shown in Fig. 6. The reaction lasted 36 hours, and the steel plates were covered with a calcium carbonate fouling layer, as shown in Fig. 7.

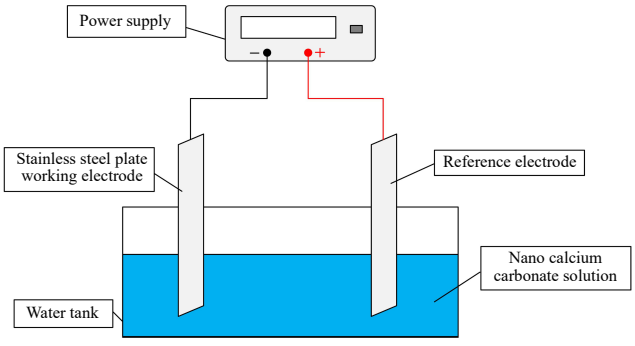

Fig. 6. Electrochemical fouling preparation system.

4.3. Descaling experiment

The descaling experiments are carried out on the steel plate covered with a fouling layer, and the system of the descaling experiment is presented in Fig. 8.

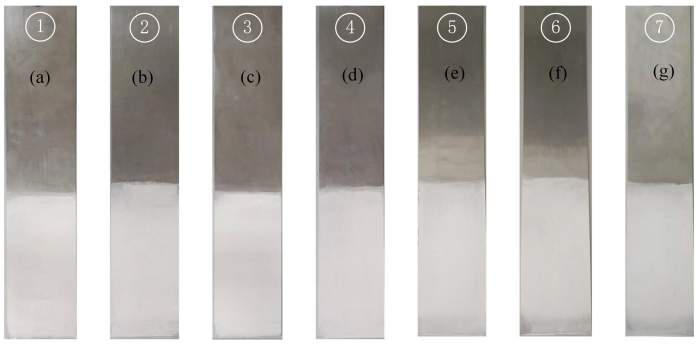

Fig. 7. Seven steel plates with calcium carbonate fouling before the descaling experiment.

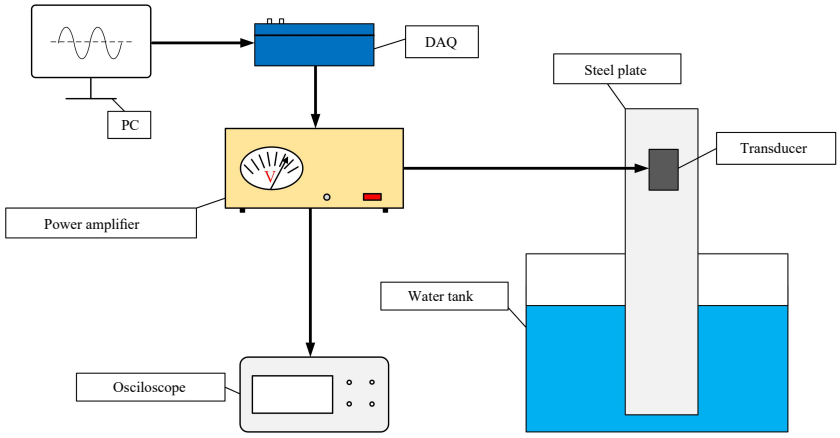

Fig. 8. System of the descaling experiment.

The digital signal is programmed by LabVIEW on a personal computer (PC) and converted into a voltage signal by a digital acquisition card (NI USB-6366). The amplitude of the voltage signal is increased to 400 V_{p-p} by the power amplifier (HFVP-83A) to drive the transducer, which converts an electrical signal into mechanical vibration based on the piezoelectric effect. In the water tank, one end of the plate covered with fouling is dipped into the water, and the transducer is attached to the other end of the plate. A single 45° beam angle transducer is used to generate UGWs in the plate.

Pressure waveforms at different frequency combinations are shown in Fig. 9. In the case of the same input amplitude, the output peak negative pressure of a dual-frequency signal is $\sqrt{2}$ times the single-frequency signal, and the output peak value of the tri-frequency signal is $\sqrt{3}$ times the single-frequency signal (Suo *et al.*, 2015).

In the following experiment, $A_0 = \sqrt{2}A_1 = \sqrt{3}A_2$ is used to ensure equal power generated between single-frequency, dual-frequency, and triple-frequency excitations. In the single-frequency descaling experiment, the input signal is a sinusoidal continuous signal:

$$s(t) = A_0 \sin(2\pi f t), \tag{9}$$

where f is the sinusoidal signal frequency: 22.480 or 36.093 or 4.437 kHz, and A_0 is the amplified amplitude of the voltage signal.

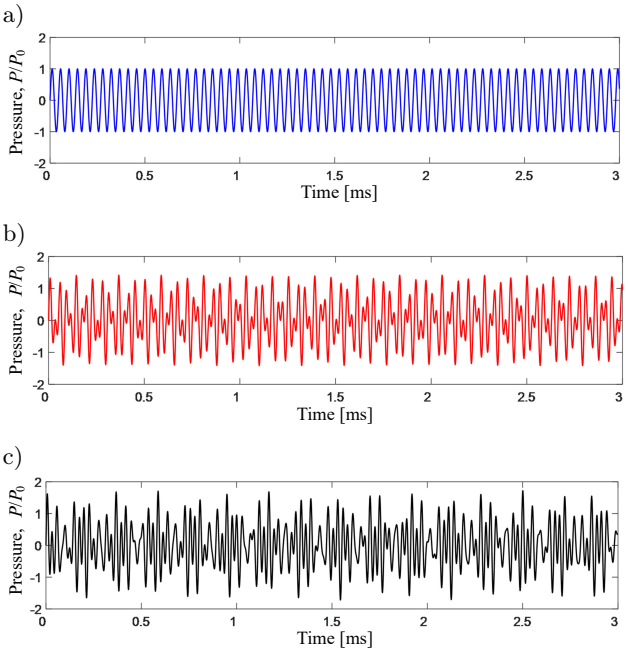

Fig. 9. Pressure waveforms at different frequency combinations: a) 22.480 kHz; b) 22.480 + 36.093 kHz; c) 22.480 + 36.093 + 41.289 kHz.

In the dual-frequency descaling experiment, the input signal is a sinusoidal dual-frequency continuous signal:

$$s(t) = A_1 \sin(2\pi f_1 t) + A_1 \sin(2\pi f_2 t), \quad (10)$$

where
f_1 = 22.480 kHz, f_2 = 36.093 kHz or f_1 = 36.093 kHz, f_2 = 41.289 kHz or f_1 = 22.480 kHz, f_2 = 41.289 kHz, and A_1 is the amplified amplitude of the voltage signal.

In the triple-frequency descaling experiment, the input signal is a sinusoidal triple-frequency continuous signal:

$$s(t) = A_2 \sin(2\pi f_1 t) + A_2 \sin(2\pi f_2 t) + A_2 \sin(2\pi f_3 t), \quad (11)$$

where
f_1 = 22.480 kHz, f_2 = 36.093 kHz, f_3 = 41.289 kHz, and A_2 is the amplified amplitude of the voltage signal.

There are seven different incentive modes in this experiment. To express the incentive modes of experiments more clearly and conveniently, different experiments are numbered, as shown in Table. 2.

Table 2. Corresponding number of different incentive modes.

Frequency [kHz]	Serial number
22.480	S1
36.093	S2
41.289	S3
36.09, 41.289	D1
22.48, 36.09	D2
22.48, 41.289	D3
22.480, 36.093, and 41.289	T1

Seven descaling results after 40 minutes of the experiment are shown in Fig. 10. Among them, the stainless steel plates numbered 1–3 show the experimental results under the excitation modes S1–S3, and the plates 4–6 show the experimental results under the excitation modes D1-D3, the case numbered 7 shows the experimental result under the excitation mode T1.

It can be seen that descaling regions show different results. Under the single-frequency excitation mode, the removed fouling area is relatively low, which indicates that the descaling effect is poor. Compared with the above single-frequency excitation mode, in the dual-frequency excitation mode, the removed fouling area accounted for a higher proportion, which shows that the descaling effect is improved. Under the three-frequency excitation mode, $CaCO_3$ fouling is eliminated, and the removed fouling area accounted for the highest proportion and the descaling effect was the best.

To quantitatively analyze the descaling result, the removal rate is introduced as:

$$\text{Removal rate} = \frac{W_r}{W_t}, \quad (12)$$

where W_r is the weight of fouling on a plate, which is removed in the descaling experiment, and W_t is the total weight of fouling in the plate before the descaling experiment.

The removal rate against time in seven descaling experiments is shown in Fig. 11.

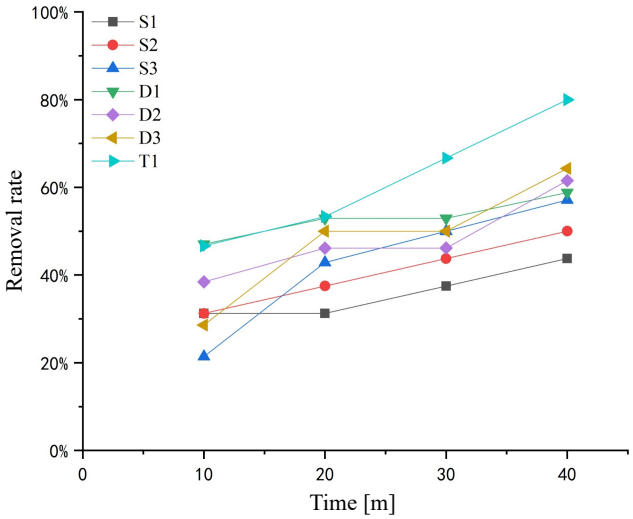

Fig. 11. Removal rate changes with time in the descaling experiment.

The removal rate in the seven experiments increased with time. However, the growth rates of descaling are different under different excitation conditions,

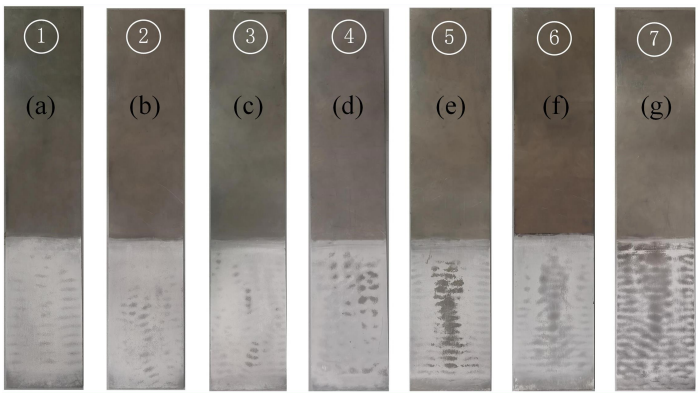

Fig. 10. Descaling results under different excitation modes: a)–c) single-frequency; d)–f) dual-frequency; g) triple-frequency.

resulting in the aliasing of the curves of the descaling rate. However, the final descaling rate showed an increasing trend from S1 to T1. Detailed data in the descaling experiments are listed in Table 3.

Table 3. Removal rate of descaling experiments.

Excitation mode	W_t [g]	W_r [g]	Removal rate [%]
S1	1.6	0.7	43.75
S2	1.6	0.8	50.00
S3	1.4	0.8	57.14
D1	1.7	1.0	58.82
D2	1.3	0.8	61.54
D3	1.4	0.9	64.29
T1	1.5	1.2	80.00

According to Table 3, the final removal rate in the triple-frequency experiment is higher than that of dual-frequency and single-frequency modes. The descaling rate of dual-frequency is higher than that of single-frequency. It can be concluded that multi-frequency excitation may improve the efficiency of descaling.

5. Discussion

This paper focuses on plate descaling methodology under multi-frequency UGWs by simulation and experiments. A numerical simulation method was used to determine the distribution of acoustic pressure on the plate under different frequency combinations. According to the simulation results, the distribution of sound pressure on the plate under triple-frequency excitation is denser and more prone to cavitation than in single-frequency and dual-frequency cases, which is beneficial for the descaling process. In the descaling experiments, the stainless steel plate is immersed in water and the UGWs propagate along the surface of the stainless steel plate. The leakage energy causes the cavitation effect on the surface of the steel plate. The experimental results show that the descaling rate under triple-frequency UGWs excitation is higher than dual-frequency, and that under dual-frequency UGWs excitation is higher than that under single-frequency. With the increase in frequency number of UGWs, the fouling removal rate on stainless steel plates is gradually improved with 40 mins removal time, and the fouling removal is more uniform. Therefore, multi-frequency UGWs excitation can improve the descaling effect.

6. Conclusion

A new descaling methodology for plate structure based on UGWs was proposed in this paper. A 45° angle beam transducer was used for descaling, and the working frequencies of the transducer under three peak values were obtained by pulse calibration. They are 22.480, 36.093, and 41.289 kHz. The descaling experiment using UGWs with single-frequency excitation showed a low descaling rate and uneven descaling. With the introduction of the second and third frequencies, the final descaling rate was higher than that of any single-frequency in the combination and the descaling rate of the triple-frequency was higher than that of the dual-frequency. Multi-frequency UGWs improve the descaling rate. This technology can be used to remove the surface dirt of steel plates in water, which is of great significance for industrial production and environmental protection.

Acknowledgments

This work was funded by the National Natural Science Foundation of China (grants no. 61873187, 62173246, and 61901299).

References

1. Abu-Zaid M. (2000), A fouling evaluation system for industrial heat transfer equipment subject to fouling, *International Communications in Heat and Mass Transfer*, **27**(6): 815–824, doi: 10.1016/S0735-1933(00)00162-7.
2. Avvaru B., Pandit A.B. (2008), Experimental investigation of cavitational bubble dynamics under multi-frequency system, *Ultrasonics Sonochemistry*, **15**(4): 578–589, doi: 10.1016/j.ultsonch.2007.06.012.
3. Chen D., Weavers L.K., Walker H.W., Lenhart J.J. (2006), Ultrasonic control of ceramic membrane fouling caused by natural organic matter and silica particles, *Journal of Membrane Science*, **276**(1–2): 135–144, doi: 10.1016/j.memsci.2005.09.039.
4. Deptuła A., Kunderman D., Osiński P., Radziwanowska U., Włostowski R. (2016), Acoustic diagnostics applications in the study of the technical condition of the combustion engine, *Archives of Acoustics*, **41**(2): 345–350, doi: 10.1515/aoa-2016-0036.
5. Feng R., Zhao Y., Zhu C., Mason T.J. (2002), Enhancement of ultrasonic cavitation yield by multi-frequency sonication, *Ultrasonics Sonochemistry*, **9**(5): 231–236, doi: 10.1016/S1350-4177(02)00083-4.
6. Gholivand Kh., Khosravi M., Hosseini S.G., Fathollahi M. (2010), A novel surface cleaning method for chemical removal of fouling lead layer from chromium surfaces, *Applied Surface Science*, **256**(24): 7457–7461, doi: 10.1016/j.apsusc.2010.05.090.
7. Habibi H. *et al.* (2016), Modelling and empirical development of an anti/de-icing approach for wind turbine blades through superposition of different types of vibration, *Cold Regions Science and Technology*, **128**: 1–12, doi: 10.1016/j.coldregions.2016.04.012.
8. Inoue D., Hayashi T. (2015), Transient analysis of leaky Lamb waves with a semi-analytical finite element method, *Ultrasonics*, **62**: 80–88, doi: 10.1016/j.ultras.2015.05.004.

9. Kim J.O., Kim J.H., Choi S. (1999), Vibroacoustic characteristics of ultrasonic cleaners, *Applied Acoustics*, **58**(2): 211–228, doi: 10.1016/S0003-682X(98)00039-5.
10. Kovarik V. (1995), Distributional concept of the elastic-viscoelastic correspondence principle, *Journal of Applied Mechanics*, **62**(4): 847–852, doi: 10.1115/1.2896010.
11. Krautkrämer J., Krautkrämer H. (2013), *Ultrasonic Testing of Materials*, 4th ed., Springer Science & Business Media, Berlin, Heidelberg.
12. Krzyzanowski M., Yang W., Sellars C.M., Beynon J.H. (2013), Analysis of mechanical descaling: and modelling approach experimental, *Metal Science Journal*, **19**(1): 109–116, doi: 10.1179/026708303225008545.
13. Kudryashova O.B., Vorozhtsov A., Danilov P. (2019), Deagglomeration and coagulation of particles in liquid metal under ultrasonic treatment, *Archives of Acoustics*, **44**(3): 543–549, doi: 10.24425/aoa.2019.129269.
14. Legay M., Allibert Y., Gondrexon N., Boldo P., Le Person S. (2013), Experimental investigations of fouling reduction in an ultrasonically-assisted heat exchanger, *Experimental Thermal and Fluid Science*, **46**: 111–119, doi: 10.1016/j.expthermflusci.2012.12.001.
15. MacAdam J., Parsons S.A. (2004), Calcium carbonate scale formation and control, *Review in Environmental Science & Bio/Technology*, **3**: 159–169, doi: 10.1007/s11157-004-3849-1.
16. Mason T.J. (2016), Ultrasonic cleaning: An historical perspective, *Ultrasonics Sonochemistry*, **29**: 519–523, doi: 10.1016/j.ultsonch.2015.05.004.
17. Mazzotti M., Marzani A., Bartoli I. (2014), Dispersion analysis of leaky guided waves in fluid-loaded waveguides of generic shape, *Ultrasonics*, **54**(1): 408–418, doi: 10.1016/j.ultras.2013.06.011.
18. Nguyen T.T., Asakura Y., Koda S., Yasuda K. (2017), Dependence of cavitation, chemical effect, and mechanical effect thresholds on ultrasonic frequency, *Ultrasonics Sonochemistry*, **39**: 301–306, doi: 10.1016/j.ultsonch.2017.04.037.
19. Pečnik B., Hočevar M., Širok B., Bizjan B. (2016), Scale deposit removal by means of ultrasonic cavitation, *Wear*, **356**: 45–52, doi: 10.1016/j.wear.2016.03.012.
20. Qu Z. *et al.* (2019), A descaling methodology for a water-filled pipe based on leaky guided ultrasonic waves cavitation, *Chemical Engineering Research and Design*, **146**: 470–477, doi: 10.1016/j.cherd.2019.04.027.
21. Rizzo F.J., Shippy D.J. (1971), An application of the correspondence principle of linear viscoelasticity theory, *SIAM Journal on Applied Mathematics*, **21**(2): 321–330, doi: 10.1137/0121034.
22. Sato H., Lebedev M., Akedo J. (2007), Theoretical investigation of guide wave flowmeter, *Japanese Journal of Applied Physics*, **46**(7S): 4521, doi: 10.1143/JJAP.46.4521.
23. Shchukin D.G., Skorb E., Belova V., Moehwald H. (2011), Ultrasonic cavitation at solid surfaces, *Advanced Materials*, **23**: 1922–1934, doi: 10.1002/adma.201004494.
24. Shima A. (1971), The natural frequencies of two spherical bubbles oscillating in water, *Journal of Fluids Engineering*, **93**(3): 426–431, doi: 10.1115/1.3425268.
25. Somerscales E.F.C. (1990), Fouling of heat transfer surfaces: An historical review, *Heat Transfer Engineering*, **11**(1): 19–36, doi: 10.1080/01457639008939720.
26. Suo D., Govind B., Zhang S., Jing Y. (2018), Numerical investigation of the inertial cavitation threshold under multi-frequency ultrasound, *Ultrasonics Sonochemistry*, **41**: 419–426, doi: 10.1016/j.ultsonch.2017.10.004.
27. Suo D., Guo S., Lin W., Jiang X., Jing Y. (2015), Thrombolysis using multi-frequency high intensity focused ultrasound at MHz range: An in vitro study, *Physics in Medicine & Biology*, **60**(18): 7403–7418, doi: 10.1088/0031-9155/60/18/7403.
28. Suslick K.S. *et al.* (1999), Acoustic cavitation and its chemical consequences, *Philosophical Transactions of the Royal Society of London. Series A: Mathematical, Physical and Engineering Sciences*, **357**(1751): 335–353, doi: 10.1098/rsta.1999.0330.
29. Wu J.-H., Chao L. (2011), Effects of entrained air manner on cavitation damage, *Journal of Hydrodynamics*, **23**(3): 333–338, doi: 10.1016/S1001-6058(10)60120-5.
30. Zhu R., Huang G.L., Huang H.H., Sun C.T. (2011), Experimental and numerical study of guided wave propagation in a thin metamaterial plate, *Physics Letters A*, **375**(30–31): 2863–2867, doi: 10.1016/j.physleta.2011.06.006.